Heliyon 10 (2024) e38082

Contents lists available at ScienceDirect

Heliyon

journal homepage: www.cell.com/heliyon

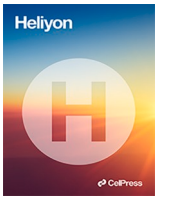

Research article

Transcriptome and RNA sequencing analysis of H9C2 cells exposed to diesel particulate matter

Kyoung Jin Nho *, Jae Hoon Shin, Jin Ee Baek, Sung Won Choi

Department of Pathogenic Laboratory Research, Institute of Occupation and Environment, Korea Workers' Compensation & Welfare Service, 478, Munemi-ro, Bupyeong-gu, Incheon, 21417, Republic of Korea

ARTICLE INFO

Keywords:
Particulate matter
Myocardium
Sequence analysis
Gene expression profiling
Gene ontology

ABSTRACT

Although air pollution has been classified as a risk factor for heart disease, the underlying mechanisms remain nebulous. Therefore, this study investigated the effect of diesel particulate matter (DPM) exposure on cardiomyocytes and identified differentially expressed genes (DEGs) induced by DPM. DPM treatment decreased H9C2 cell viability and increased cytotoxicity. Ten genes showed statistically significant differential expression following treatment with DPM at 25 and 100 μg/ml for 3 h. A total of 273 genes showed statistically significant differential expression following treatment with DPM at 25 and 100 μg/ml for 24 h. Signaling pathway analysis revealed that the DEGs were related to the 'reactive oxygens species,' 'IL-17,' and 'fluid shear stress and atherosclerosis' signaling pathways. *Hmox1*, *Fos*, and *Fosb* genes were significantly upregulated among the selected DEGs. This study identified DPM-induced DEGs and verified the selected genes using qRT-PCR and western blotting. The findings provide insights into the molecular events in cardiomyocytes following exposure to DPM.

1. Introduction

World Health Organization (WHO) reported approximately 18 million deaths worldwide attributed to cardiovascular disease (CVD) every year [1]. This accounts for approximately 30 % of all deaths and corresponds to a high rate of morbidity and mortality. This increasing trend is highly correlated with lifestyle factors, such as population aging, westernized eating habits, smoking, and alcohol consumption; however, recent studies have shown that environmental factors, such as air pollution, play an essential role in inducing and exacerbating CVD [2,3]. Although all components of air pollution harm health, the relationship between fine dust, or particulate matter (PM), in the air and CVD has been well established [3,4]. However, previous research has focused on cohort analyses and clinical investigations; therefore, data on the mechanism linking heart disease to PM exposure remain limited.

PM is divided into fine dust (<10 μm, PM_{10}), ultrafine dust (<2.5 μm, $PM_{2.5}$), and ultrafine particles (<0.1 μm, $PM_{0.1}$), depending on the particle size [5,6]. Diesel particulate matter (DPM), which is classified as $PM_{2.5}$, was upgraded to a Group 1 carcinogen by the International Agency for Research on Cancer (IARC), and DPM has been classified as a substance that causes lung cancer [7]. DPM

Abbreviations: WHO, World Health Organization; CVD, cardiovascular disease; DPM, diesel particular matter; DEG, differentially expressed gene; PM, particulate matter; IARC, International Agency for Research on Cancer; PAH, polycyclic aromatic hydrocarbon; IEG, immediate early response gene; NIST, National Institute of Science and Technology; ERM, European Reference Materials; PPI, protein-protein interactions; PDI, poly diversity index.

* Corresponding author.
E-mail address: nkj1130@comwel.or.kr (K.J. Nho).

https://doi.org/10.1016/j.heliyon.2024.e38082
Received 18 June 2024; Received in revised form 19 August 2024; Accepted 17 September 2024
Available online 18 September 2024

represents a complex composed of various substances, such as organic carbon, elemental carbon, sulfate, nitroarenes, and polycyclic aromatic hydrocarbons (PAHs). The composition of DPM varies based on the fuel, exhaust system, and engine type. Due to the small particle size, DPM remains in the air for a long time and has harmful health effects [8]. Indeed, DPM causes severe respiratory damage and lung diseases, such as asthma, pulmonary fibrosis, and chronic obstructive pulmonary disease [9–11]. However, recent reports have indicated that the causal relationship between DPM ($PM_{2.5}$) and mortality is stronger in heart disease than respiratory disease [12–14]. Previous studies have also reported that PM in air pollutants induces a strong oxidative stress response in the respiratory tract following inhalation. This oxidative stress is increased by stimulating enzymatic reactions in various pathways and ultimately induces a systemic vascular oxidative stress response, causing CVD [15–17]. Air pollution is composed of complex mixtures of gases and solid substances; however, its effects are primarily attributed to organic compounds, such as PM and PAHs, bound to the surface of PM [18, 19].

Data on the biological pathways associated with PM and CVD are lacking; however, previous studies have suggested the involvement of autonomic nervous system imbalance, systemic outflow of inflammatory mediators, and systemic transport of organic compounds [14,16,20]. Research on the biological pathways involved in CVDs has mainly focused on vascular endothelial cells [21–24]. Increased exposure to atmospheric PM exacerbates oxidative stress and generates high concentrations of reactive oxygen species (ROS) that interfere with calcium circulation in the myocardium and induce cell death [25–27]. However, molecular mechanism studies of the effects of PM on myocardial cells, particularly on differential gene expression, are lacking. Therefore, this study evaluated the toxicity of DPM in H9C2 cardiomyocyte cells, identified the genes regulated by DPM, and analyzed the network of selected genes.

2. Materials and methods

2.1. Reagents and materials

The plastic materials used in the experiments were purchased from Corning Inc. (Corning, NY, USA) and BD Falcom LabWare (NJ, USA). The phosphate-buffered saline (PBS) used for sample dispersion was purchased from Gibco (NY, USA), and the reagents used in the experiment were purchased from Sigma Aldrich (MO, USA).

2.2. Cell culture

H9C2 cells were purchased from ATCC (Manassas, VA, USA) and cultured according to the manufacturer's instructions. Cells were cultured in Dulbecco's Modified Eagles Medium (DMEM, ATCC) with 10 % FBS (ATCC) and 1 % penicillin-streptomycin (Gibco/BRL, Grand Island, NY, USA) and incubated in a humidified environment at 5 % CO_2 and 37 °C.

2.3. Sample preparation and treatment

Four types of PM were obtained from the National Institute of Science and Technology (NIST) and European Reference Materials (ERM). The experiment used two types of PM_{10} (ERM-CZ100 and ERM-CZ120) and $PM_{2.5}$ (SRM1650b and SRM2975). The material properties are specified in the certificates provided by each manufacturer. The four types of particulate matter were suspended in PBS and stored at 10 mg/ml until use. The stock solution was diluted with DMEM and sonicated for 1 h in an ultrasonic bath to effectively disperse particulate matter. Sample information is presented in Table S1.

2.4. Cell viability assay

Cell viability was assessed using a Cell Counting Kit 8 (CCK-8) assay (Dojindo Molecular Technologies, Inc., Rockville, MD, USA). The cells were plated in a 96-well plate and exposed to four types of particulate matter at various concentrations. Following a 24-h incubation, the CCK-8 solution was added to each well and reacted at 37 °C. Absorbance was measured at 450 nm using a microplate reader (Tecan Group Ltd., Tokyo, Japan). Cell viability was expressed as a percentage of the absorbance of the untreated control cells.

2.5. Cell toxicity assay

Cell toxicity was assessed using an LDH assay kit following the guidelines (Dojindo Molecular Technologies, Inc.). The cells were seeded in a 96-well plate and treated with the four PM types of particulate matter at various concentrations. Subsequently, the culture medium was transferred to a new 96-well plate and reacted with the LDH reagent, and the reaction was terminated by adding a stop solution. The absorbance was measured at 490 nm using a microplate reader (Tecan). Cytotoxicity was measured as a percentage of the absorbance of the untreated control cells.

2.6. Characterization of SRM1650b

The morphology of SRM1650b was assessed using transmission electron microscopy (TEM, Hitachi H-7650, UK). The particle size and dispersion stability of SRM1650b in the solvent were measured using a Zetasizer Nano ZS90 (Malvern Instruments, UK).

2.7. RNA isolation and RNA sequencing

RNA sequencing (RNA-Seq) is an analytical method used to measure transcript expression using next-generation sequencing (NGS) and can confirm the diversity of gene expression between cells and the uniqueness of each cell type. Therefore, RNA-Seq can identify genes with variations in expression under different conditions, identify new genes, and determine their interactions [28,29]. We performed RNA-seq to identify differentially expressed genes (DEGs) following SRM1650b treatment. Cells were exposed to SRM1650b at 25 and 100 μg/ml for 3 and 24 h, and total RNA was then extracted from both the control and SRM1650b-treated cells using a PureLink™ RNA mini kit (Invitrogen, USA) according to the manufacturer's instructions. RNA quality was evaluated using an Agilent TapeStation 4000 system (Agilent Technologies, NL, CA, USA), and RNA was quantified using an ND-2000 Spectrophotometer (Thermo Fisher Scientific, Waltham, MA, USA). QuantSeq 3′ mRNA-Seq analysis was conducted at Ebiogen (Seoul, Korea). The QuantSeq 3′ mRNA Seq Library Prep Kit (Lexogen, Inc., Austria) was used to generate libraries from the control and test RNAs following the manufacturer's instructions. In summary, total RNA was prepared and reverse-transcribed using oligo-dT. The RNA template was digested, and a random primer was added to the 5′ end to synthesize the second strand. Double-stranded libraries were filtered and amplified to contain all adapter sequences required for cluster generation. The completed library was subjected to high-throughput sequencing using NextSeq 550 (Illumina, Inc., USA) [30].

2.8. Data collection and differentially expressed gene analysis

The mRNA sequencing data was assessed using the Excel-based DEG (ExDEGA) analysis tool provided by Ebiogen. In a concise overview, QuanSeq 3' mRNA-Seq reads were aligned using Bowtie2 [31]. Aligned reads were used to assemble the transcripts, confirm the expression levels, and identify DEGs. DEGs were identified based on counts from both unique and multiple alignments using coverage in bedtools [32]. Read count data were processed via the transcripts per million (TPM) and counts per million (CPM) normalization method using EdgR. DEGs in SRM1650b-treated cells were analyzed based on a significance threshold of p-value$<$0.05, fold change (FC)$\geq$2, and normalized data (log2) = 2 relative to DEGs from SRM1650b-untreated cells. The identified genes were represented in a heatmap and organized through hierarchical clustering. ExDEGA (Ebiogen Inc., Korea) was used to mine data and create graphical representations.

2.9. Gene ontology and functional enrichment analysis

Gene Ontology (GO) functional enrichment analysis was performed to identify the functions of DEGs according to GO terms, namely biological processes (BPs) and molecular functions (MFs). Gene functions and signaling pathways were analyzed using the Database for Annotation, Visualization, and Integrated Discovery (DAVID, https://david.ncifcrf.gov/) and the Kyoto Encyclopedia of Genes and Genomes (KEGG, https://www.genome.jp/kegg/). The relationships between DEGs and biological signaling pathways were analyzed using the KEGG database. The STRING website (functional protein association networks (string-db.org)), which provides a biological database and anticipated protein-protein interactions (PPIs), was used to analyze the functional protein association networks of the selected genes. Genes were analyzed with a cutoff p-value$<$0.05 and FC $\geq$ 2. Data were collected and visualized using the ExDEGA software (Ebiogen Inc., Seoul, Korea).

2.10. Quantitative real-time PCR (qRT-PCR) validation

Total RNA was isolated using a PureLink RNA Mini Kit (Invitrogen, Waltham, USA) and quantified using a Nabi nano spectrophotometer (MicroDigital Co., Korea). Complementary DNA (cDNA) was synthesized by reverse transcription from 1 μg of total RNA using a High Capacity RNA to cDNA kit (ABI, Waltham, USA). The synthesized cDNA was used as a template, and qRT-PCR was performed using the primers listed in Table S2 mRNA expression was normalized to that of 18s rRNA, and the expression level was measured using the comparative Ct method. All experiments were performed in triplicate.

2.11. Protein isolation and western blotting validation

For protein isolation, cells were homogenized with PRO-PREP protein extraction solution (Intron Biotechnology, Korea) and centrifuged to separate the supernatant. Total protein was quantified using a BCA protein assay kit (Pierce, MA, USA), and 10–30 μg protein was subjected to SDS-PAGE on a 10–20 % polyacrylamide gel. The membranes were blocked with 5 % bovine serum albumin in TBST for 1 h. Primary antibody was then added and incubated overnight at 4 °C. On the following day, the membrane was washed thrice with TBST and incubated with the secondary antibody for 1 h at 20–22 °C. The membrane was washed with TBST and assessed using an Amersham Imager 600 (GE Healthcare, MA, USA). To analyze the results, bands were quantified using NIH ImageJ software, and values for the target protein were normalized to that of glyceraldehyde 3 phosphate dehydrogenase (GAPDH). Uncropped gel images are shown in Fig. S3.

2.12. Measurement of ROS generation

Intracellular ROS levels were assessed using the DCFDA/H2DCFDA Cellular ROS assay kit following the manufacturer's instructions (Abcam, UK). SRM1650b-treated and untreated cells were loaded with 20 μM DCFDA solution for 45 min at 37 °C in the

dark. Subsequently, the cells were washed twice with PBS before analysis using a microplate (Tecan) for immediate fluorescence measurements at 485/535 nm (Ex/Em). An Axio Imager M2 microscope (Carl Zeiss, Oberkochen, DE) equipped with an FITC filter set was used to detect ROS generation, and visual assessment of cell brightness was conducted and compared between the control and sample groups. Analysis was performed using Zeiss ZEN 3.7 software (Carl Zeiss).

2.13. Measurement of mitochondrial membrane potential

Quantified changes in the mitochondrial membrane potential in live cells were measured using the TMRE-MMP assay kit according to the manufacturer's instructions (Abcam, UK). Cells were treated with SRM1650b for 24 h, and 300 nM TMRE solution was added for 15 min in the dark. The cells were washed twice with PBS before analysis using a microplate reader and fluorescence microscope. The cells were immediately analyzed using a fluorescence microplate reader at 549/575 nm (Ex/Em) and microscopy with a rhodamine filter set. The cells were visually scored for brightness, and the control and samples were compared. Analysis was performed using Zeiss

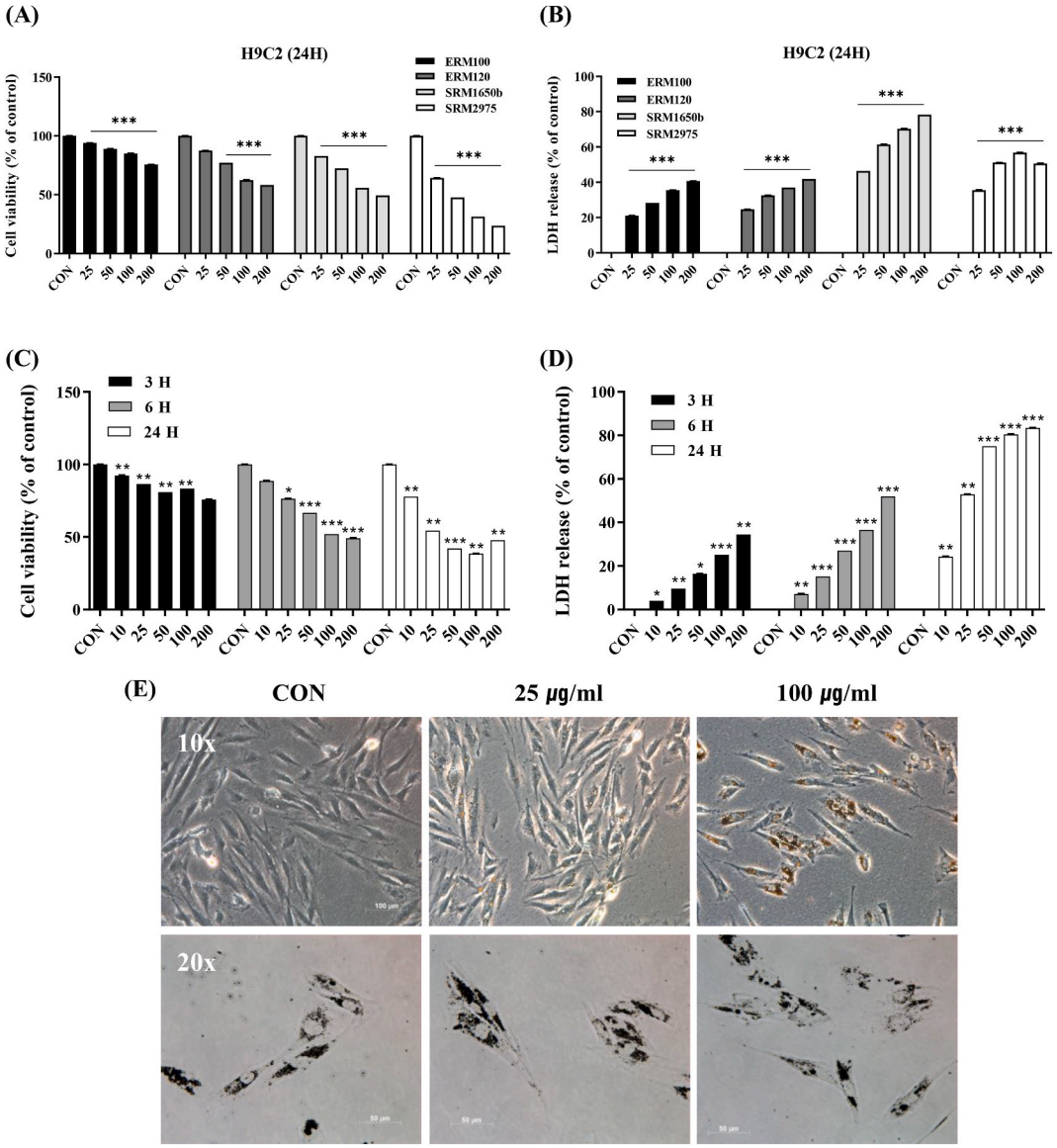

Fig. 1. Cell viability and toxicity of four types of PM in H9C2 cells. H9C2 cells were treated with four types of PM for 24 h at several concentrations (25–200 μg/ml). (A) Cell viability was assessed using CCK-8 assay. (B) Cell toxicity was assessed using LDH assay. Cells were treated with various concentrations of SRM1650b for 3, 6, and 24 h. (C) Cell viability was assessed using CCK-8 assay. (D) Cell toxicity was assessed using LDH assay. Data are expressed as the means ± SD of triplicate samples. *p-value<0.05, **p-value<0.01 and *** p-value<0.001 *vs.* untreated PM. (E) Cell morphology was detected using an inverted microscope. Upper panel; 10× and low panel; 20× magnification. Scale bar = 50 and 100 μm.

ZEN 3.7 software.

2.14. Statistical analysis

Statistical analyses were performed using Prism 5 software (GraphPad, San Diego, CA, USA). Data are represented as the mean ± standard deviation (SD). Unpaired *t*-tests were used to evaluate statistically significant differences between two groups, and one-way analysis of variance (ANOVA) with Dunnett's test was used to assess differences among multiple groups. Statistical significance was set at $p < 0.05$.

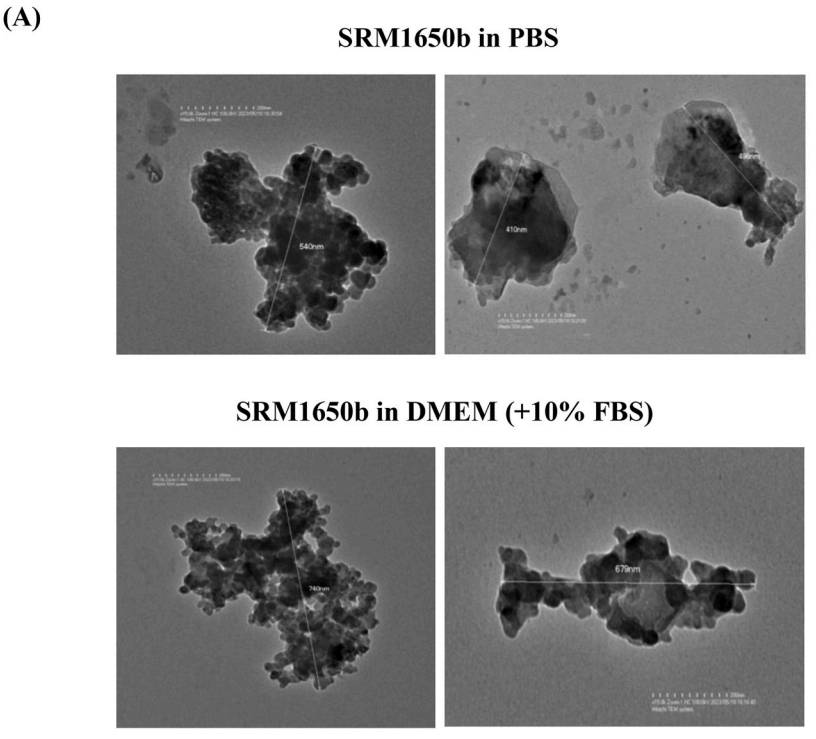

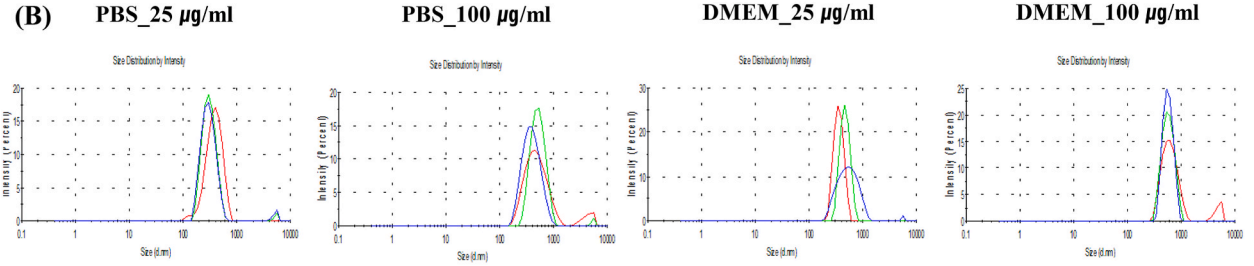

Sample	Diameter (nm)	PDI	Zeta-potential (mV)
PBS_25	354.3 ± 73.42	0.278 ± 0.106	-35.6 ± 1.11
PBS_100	452.1 ± 79.56	0.22 ± 0.062	-35.5 ± 4.88
DMEM_25	523.0 ± 91.76	0.310 ± 0.044	-28.7 ± 4.31
DMEM_100	614.0 ± 70.66	0.203 ± 0.138	-27.1 ± 4.60

Fig. 2. Morphological characterization of SRM1650b. (A) Representative TEM images of SRM1650b suspended in PBS and DMEM (+10 % FBS). ×15.0 k magnification, Scale bar = 200 nm. (B) Size distribution and zeta potential of SRM1650b suspended in PBS and DMEM (+10 % FBS) were measured using a Zeta sizer. n = 3.

3. Results

3.1. Effects of PM on H9C2 cells

We first examined the effects of four PM types on H9C2 cell viability and toxicity. The PM information is listed in Table S1. The H9C2 cells were exposed to several concentrations of the four PMs (25, 50, 100, and 200 μg/ml) for 24 h. Cell viability and toxicity were measured using CCK-8 and LDH assays. The four PM types reduced the cell viability in a concentration-dependent manner (Fig. 1A). In contrast, cell toxicity increased in a concentration-dependent manner (Fig. 1B). The results showed that $PM_{2.5}$ led to a more significant increase in cell toxicity than PM_{10}. Furthermore, as the size of particulate matter decreases, cell viability decreases, and cytotoxic effects increase. In particular, SRM1650b, a representative DPM substance classified as $PM_{2.5}$, was used in this experiment as it showed the greatest cytotoxic effect on H9C2 cells. SRM1650b was added at various concentrations and times, and cell viability and toxicity were measured. After treatment, the cell viability decreased in a concentration- and time-dependent manner (Fig. 1C) while the cytotoxic effects increased (Fig. 1D). The cells' shape changed to radial (Fig. 1E). Additionally, we speculated that SRM1650b was deposited around the nucleus, thereby affecting cell viability.

3.2. Characterization of SRM1650b

The morphology of SRM1650b was examined using TEM, and the particle size and dispersion were measured using a Zetasizer. TEM revealed that SRM1650b showed irregular shapes in both PBS and DMEM (+10%FBS), with small particles agglomerating to form single granules (Fig. 2A). The particle size ranged from 354.3 ± 73.42 nm to 452.1 ± 79.56 nm for samples dispersed in PBS and from 523.0 ± 91.76 nm to 614 ± 70.66 nm for samples dispersed in DMEM containing 10 % FBS (Fig. 2B). Additionally, the zeta potential data showed that SRM1650b had a significant negative charge in PBS and DMEM (Fig. 2B). This is probably because in biological contexts, a protein corona forms on the surface of particles [33]. The particle size and zeta potential values changed based on the SRM1650b concentration and suspension type. Our data showed that the particle size and zeta potential values tended to increase more in samples suspended in DMEM than in PBS. However, the SRM1650b certificate stated that the size of the SRM1650b particles was <2.5 μm; based on the actual measured results, the particles were distributed at < 1 μm. The poly diversity index (PDI), which refers to the size dispersion of the particles, was <0.3 (Fig. 2B), indicating that the SRM1650b particles were relatively evenly distributed in the suspension.

3.3. Identification of differentially expressed genes

To identify genes expressed caused by SRM1650b treatment, H9C2 cells were treated with SRM1650b at concentrations of 25 and 100 μg/ml for 3 and 24 h. RNA from each group was extracted, and RNA sequencing was performed. Group separation and data analysis are illustrated in Fig. S1. Before DEG analysis, principal component analysis (PCA) was performed based on the expression values of all genes in the samples to confirm expression similarity between samples. The PCA results showed that the same groups, which were grouped well, showed similar expression (Fig. S2A); therefore, a hierarchical clustering heat map was created to determine the similarity between the samples and genes. The upper dendrogram of each heatmap indicates expression similarity between samples, and the left dendrogram indicates expression similarity between genes (Fig. S2B). DEGs were aligned using bedtools and analyzed (p-value$<$0.05, FC $\geq$ 2). In the SRM1650b 3 h treatment group, a total of 12 genes showed statistically significant expression at a concentration of 25 μg/ml (SRM-25 μg/ml), while 50 showed statistically significant expression at a concentration of 100 μg/ml (SRM-100 μg/ml) compared with the control group (Fig. S2C). In the group treated with SRM1650b for 24 h, a total of 428 genes showed significant expression at a concentration of SRM-25 μg/ml, while 1214 showed significant expression at a concentration of SRM-100 μg/ml (Fig. S2C). This indicates that changes in the gene network within cardiomyocytes due to SRM1650b exposure may occur in a concentration- and time-dependent manner.

3.4. Transcriptomic analysis of SRM1650b-treated H9C2 cells (3 h)

To investigate the detailed biological changes, we first analyzed DEGs in the SRM1650b 3 h treatment group. In the SRM-25 and -100 μg/ml treatment groups, 10 genes in common showed statistically significant differential expression (p-value$<$0.05, FC $\geq$ 2, log2 = 2) (Fig. 3), of which 8 were upregulated and 2 were downregulated (Table 1). Based on these 10 genes, the expression similarity between the samples and genes was analyzed using a heatmap (Fig. 3B). We also analyzed the 10 DEGs based on GO term and signaling pathway enrichment using the DAVID and KEGG online databases. GO terms were enriched in biological process (BP) and molecular function (MF) categories. The top 10 BP terms were related to positive regulation of pri-miRNA transcription from RNA polymerase II promoter, transcription from RNA polymerase II promoter, myoblast proliferation, negative regulation of cell proliferation, and cellular response to cadmium ions, as shown in Fig. 3C and Table S3. The top 10 MF terms were related to double-stranded DNA binding, transcription factor activity, RNA polymerase II transcription factor activity, RNA polymerase II core promoter proximal region sequence-specific DNA binding, and sequence-specific DNA binding, as shown in Fig. 3C and Table S4. Most of these highly impacted GO terms appeared to be involved in the response to SRM1650b stimulation, indicating that the cells modified their metabolism drastically in response to SRM1650b. Six KEGG pathways were significantly changed at the $p < 0.05$ level (Fig. 3C and Table S5). Overall, the pathway analysis demonstrated a cellular response centered along the axes of ROS, immune processes, and fluid shear stress/atherosclerosis. We also analyzed the protein-protein interaction (PPI) network of 10 genes using the STRING online tool.

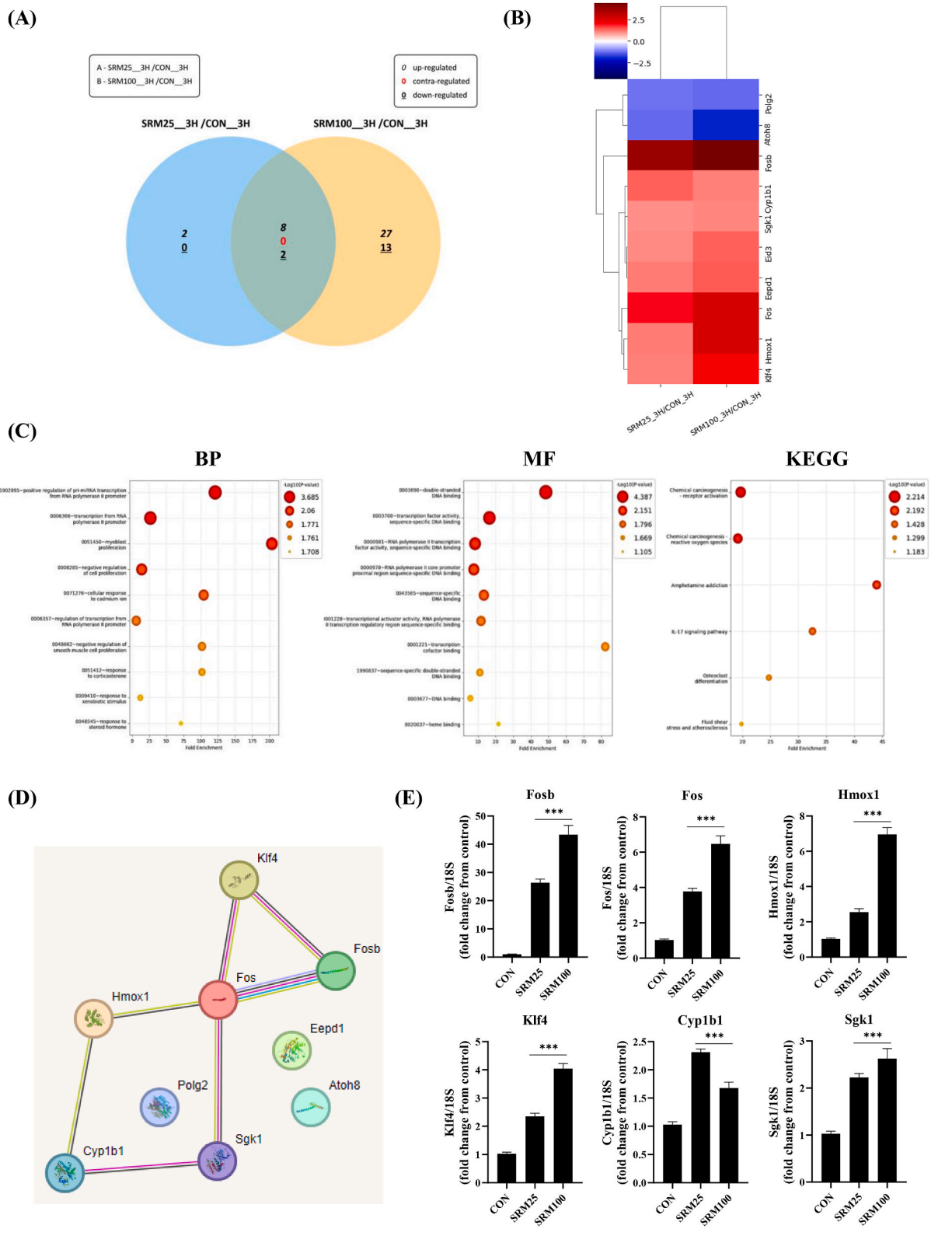

(caption on next page)

Fig. 3. Transcriptome analysis following treatment with SRM1650b for 3 h. (A) Differentially expressed genes between the CON and STM1650b 3 h-treated groups on the Venn diagram. (B) Heat map representing hierarchical clustering of 10 differentially expressed genes by treated SRM1650b for 3 h. (C) Gene Ontology analysis of 10 differentially expressed genes between the CON and SRM 3 h-treated group. BP; biological process, MF; molecular function. (D) PPI analysis of 10 differentially expressed genes from the SRM1650b 3 h treatment group. (E) Validation of selected gene expression level using qRT-PCR. Bar graph expressed as the means ± SD of triplicate samples. *** p-value < 0.001 *vs.* CON (untreated SRM1650b).

Table 1
10 DEGs in SRM1650b 3 h treatment groups.

Gene: 10		Fold change		p-value		Average of normalized data (log2)		
ID	**symbol**	**SRM25/CON**	**SRM100/CON**	**SRM25/CON**	**SRM100/CON**	**CON**	**SRM25**	**SRM100**
480	Fosb	14.074	21.740	0.000	0.000	2.164	5.979	6.606
13567	Fos	3.900	6.512	0.000	0.000	4.603	6.567	7.306
7602	Hmox1	2.309	6.431	0.000	0.000	8.111	9.318	10.796
12375	Klf4	2.255	4.249	0.000	0.000	5.796	6.969	7.883
15019	Eepd1	2.305	2.756	0.014	0.006	1.626	2.830	3.088
14079	Eid3	2.082	2.672	0.001	0.010	1.772	2.830	3.190
13120	Cyp1b1	2.640	2.219	0.000	0.018	1.669	3.070	2.819
101	Sgk1	2.039	2.134	0.001	0.002	7.408	8.436	8.501
3542	Polg2	0.439	0.404	0.002	0.000	2.544	1.356	1.238
11511	Atoh8	0.412	0.251	0.000	0.000	4.319	3.038	2.324

p-value<0.05; FC ≥ 2; log2 = 2, red box, upregulated; blue box, downregulated.

PPI analysis revealed a network with nine nodes and seven edges (Fig. 3D). Among the genes in the network, the expression of six network organically interacting genes (*Fosb, Fos, Hmox1, Klf4, Cyp1b1,* and *Sgk1*) was validated using qRT-PCR (Fig. 3E). The expression pattern was similar to that observed in the DEG analysis.

3.5. Transcriptomic analysis of SRM1650b-treated H9C2 cells (24 h)

We analyzed the transcriptome of the SRM1650b 24 h treatment group compared with that of the control group. In the SRM-25 and -100 μg/ml treatment groups, 273 genes in common showed significant differential expression (p-value<0.05, FC ≥ 2, log2 = 4), of which 82 were upregulated and 191 downregulated (Fig. 4A). Based on these 273 genes, the expression similarity between the samples and genes was analyzed using a heatmap (Fig. 4B). We selected the top 20 upregulated DEGs sorted by fold change and performed GO analysis (Table 2 and Fig. 4C). The top seven GO terms in the BP category were related to the response to xenobiotic stimulus, aging, oxidative stress, estradiol, transcription from the RNA polymerase II promoter, lipopolysaccharide, and cellular response to oxidative stress, as shown in Fig. 4C and Table S6. The top 10 terms in the MF category were related to the responses to double-stranded DNA binding, identical protein binding, protein homodimerization activity, transcription cofactor binding, and sequence-specific DNA binding, as shown in Fig. 4C and Table S7. Eight KEGG pathways were significantly altered ($p < 0.05$; Fig. 4C and Table S8). PPI analysis revealed a network with 20 nodes and 27 edges (Fig. 4D). Among the genes in the network, the expression of five organically interacting genes (*Nqo1*, *Gsta1*, *Spstm1*, *Hmox1*, and *Fos*) was related to fluid shear stress and the atherosclerosis signaling pathway. Moreover, three organically interacting genes (*Fos*, *Fosb*, and *Cxcl1*) were involved in the IL-17 signaling pathway. The expression of eight organically interacting genes was validated using qRT-PCR (Fig. 4E). The expression pattern was similar to that observed in the DEG analysis.

3.6. Validation of co-expressed genes following SRM1650b treatment for 3 and 24 h

We analyzed the five co-expressed DEGs (*Fos, Fosb, Hmox1, Klf4,* and *Eepd1*) in the SRM1650b 3 and 24 h treatment groups. PPI analysis revealed a network with five nodes and four edges (Fig. 5A). Among the genes in the network, the expression of three organically interacting genes (*Hmox1*, *Fos*, and *Fosb*) was significantly related to fluid shear stress, atherosclerosis, IL-17, and oxidative stress response pathways. The expression of the three organically interacting genes was validated using qRT-PCR (Fig. 5B) and Western blot analyses (Fig. 5C). The RNA and protein expression patterns were similar to those of the DEG analysis. A strong correlation was observed between the RNA sequencing data and qRT-PCR and Western blot analysis results. This affirms the reliability of the RNA sequencing results in this study.

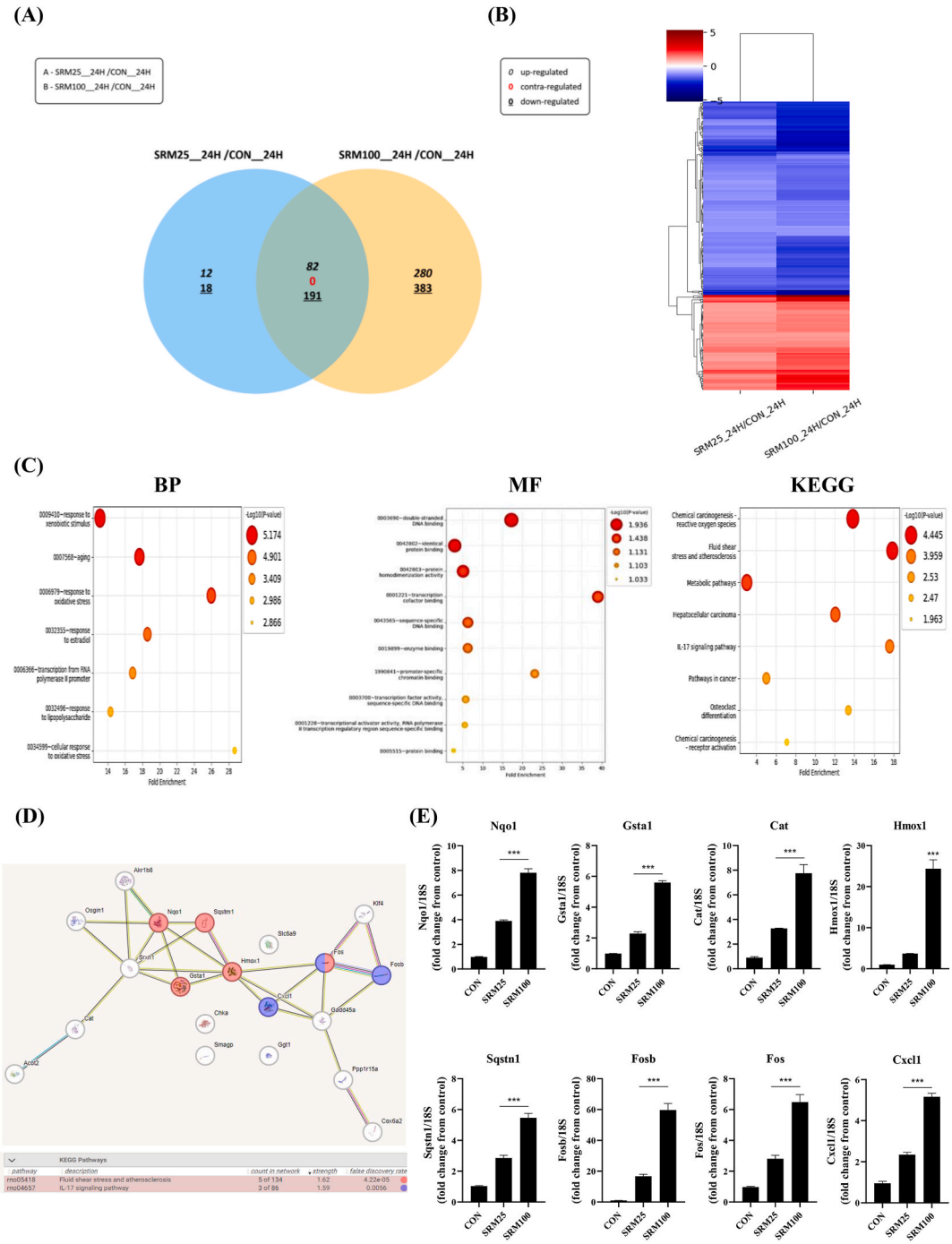

Fig. 4. Transcriptome analysis following treatment SRM for 24 h. (A) Differentially expressed genes between the CON and STM 24 h-treated groups on the Venn diagram. (B) Heat map representing hierarchical clustering of 273 differentially expressed genes treated with SRM for 24 h. (C) Gene Ontology analysis of differentially expressed genes between the CON and SRM 24 h-treated group. BP, biological process; MF, molecular function. (D) PPI analysis of the top 20 upregulated differentially expressed genes from the SRM1650b 24 h treatment group. (E) Validation of selected gene expression level using qRT-PCR. Bar graph expressed as the means ± SD of triplicate samples. *** p-value < 0.001 *vs.* CON (untreated SRM1650b).

3.7. Measurement of ROS generation and mitochondria membrane potential

Our results showed that six selected DEGs (*Fos*, *Hmox1*, *Cyp1b1*, *Klf4*, *Nqo1*, and *Cat*) were highly associated with the oxidative stress response pathway. Therefore, we measured intracellular oxidative stress using fluorescence microscopy and a microplate reader.

Table 2
Top 20 upregulated DEGs in the SRM1650b 24 h treatment groups.

110		Fold change		p-value		Average of normalized data (log2)		
ID	symbol	SRM25/CON	SRM100/CON	SRM25/CON	SRM100/CON	CON	SRM25	SRM100
480	Fosb	11.553	39.579	0.003	0.000	0.820	4.350	6.127
7870	Osgin1	11.014	39.355	0.001	0.000	1.325	4.787	6.624
7602	Hmox1	4.215	22.888	0.000	0.000	7.319	9.395	11.836
9388	Ggt1	7.635	19.334	0.001	0.000	1.686	4.619	5.959
11262	Akr1b8	3.224	11.314	0.001	0.000	5.401	7.090	8.901
10301	Cat	3.637	8.969	0.000	0.000	4.783	6.646	7.948
7791	Nqo1	3.835	8.036	0.000	0.000	8.269	10.209	11.276
13567	Fos	2.838	7.650	0.000	0.000	3.747	5.252	6.683
5307	Cxcl1	2.437	6.781	0.002	0.000	5.515	6.800	8.277
12375	Klf4	2.502	5.920	0.001	0.000	5.335	6.658	7.900
11488	Gadd45a	3.030	5.837	0.000	0.000	7.111	8.711	9.657
12624	Slc6a9	3.003	5.701	0.000	0.000	4.028	5.615	6.539
821	Ppp1r15a	2.196	5.575	0.001	0.000	6.182	7.317	8.661
16009	Gsta1	2.281	5.538	0.001	0.000	3.567	4.757	6.037
1549	Cox6a2	3.935	5.234	0.001	0.000	3.609	5.586	5.997
10669	Srxn1	2.117	5.164	0.000	0.000	5.594	6.676	7.963
13533	Acot2	2.494	5.085	0.001	0.000	5.710	7.029	8.057
2639	Sqstm1	2.601	4.695	0.000	0.000	8.338	9.717	10.569
14753	Smagp	3.989	4.672	0.000	0.000	2.163	4.159	4.387
1750	Chka	2.029	4.420	0.006	0.000	3.164	4.185	5.308

p-value<0.05; FC ≥ 2; log2 $= 4$.

H9C2 cells were stimulated with SRM1650b and H_2O_2 (positive control) loaded with DCFDA and observed under a fluorescence microscope using an FITC filter. As shown in Fig. 6A, ROS levels increased in the SRM1650b treated group. The microplate reader results also showed increased fluorescence intensity in cells exposed to SRM1650b (Fig. 6B). This indicates that exposure to SRM1650b causes intracellular ROS generation. This increase in intracellular ROS levels induces oxidative stress in the mitochondria, resulting in DNA damage and cell death. Therefore, we examined the role of SRM1650b in regulating the mitochondrial oxidative stress response. H9C2 cells were treated with SRM1650b, followed by an analysis of the mitochondrial membrane potential by TMRE staining. The mitochondrial membrane potential was significantly depolarized in the SRM1650b treated group, as shown by fluorescence microscopy (Fig. 6C) and a microplate reader (Fig. 6D). The mitochondrial uncoupler carbonyl cyanide 4-trifluoromethoxy phenylhydrazone (FCCP) was used as a negative control to depolarize the mitochondria. These results suggest that SRM1650b increases ROS levels in H9C2 cells and inhibits mitochondrial activity, thereby contributing to H9C2 cell toxicity.

4. Discussion

This study investigated the effects of diesel particulate matter on H9C2 cells and analyzed DEGs by DPM using RNA sequencing. The results confirmed that H9C2 cells treated with SRM1650b ($PM_{2.5}$) showed decreased cell viability and cytotoxicity was induced in a concentration- and time-dependent manners (Fig. 1). Additionally, an analysis of DEGs following SRM1650b treatment confirmed that Cyp1b1, Klf4, Nqo1, Gsta1, Cat, Hmox1, Fos, Sqstm1, Cxcl1, and Fosb were significantly induced by SRM1650b treatment. These genes are involved in the ROS (https://www.genome. jp/pathway/rno05208), fluid shear stress/atherosclerosis (https://www.genome.jp/pathway/rno05418), and IL-17 signaling (https://www.genome.jp/pathway/rno04657) intracellular pathways. In particular, genes involved in the ROS pathway were upregulated. Among them, the significant upregulation of Hmox1 was based on the significant oxidative stress in H9C2 cells caused by SRM1650b. Hmox1 is a typical oxidative stress marker and isoform encoding HO-1 [34,35], a crucial inducible defense molecule activated in response to oxidative stress [36,37]. Oxidative stress can increase ROS levels in affected cells. Increased ROS levels in heart disease are closely related to myocardial infarction, vascular dysfunction, and apoptosis [38–40]. Recent studies have reported that increased exposure to fine dust increases oxidative stress, with high concentrations of ROS causing cell death and disrupting calcium circulation in the myocardium [26,41]. Our data showed that SRM1650b induced ROS generation in H9C2 cells and the overexpression of Hmox1, which is involved in oxidative stress (Figs. 5 and 6). Additionally, intracellular ROS generation decreased the mitochondrial membrane potential (Fig. 6). DPM increases oxidative stress in endothelial tissues and induces

(A)

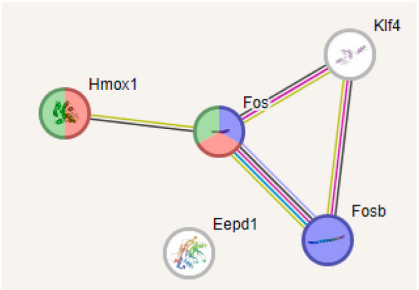

KEGG Pathways				
pathway	description	count in network	strength	false discovery rate
rno05031	Amphetamine addiction	2 of 60	2.17	0.0252
rno04657	IL-17 signaling pathway	2 of 86	2.01	0.0255
rno04380	Osteoclast differentiation	2 of 110	1.91	0.0275
rno05418	Fluid shear stress and atherosclerosis	2 of 134	1.82	0.0304

WikiPathways				
pathway	description	count in network	strength	false discovery rate
WP173	Oxidative stress response	2 of 21	2.63	0.0013

(B)

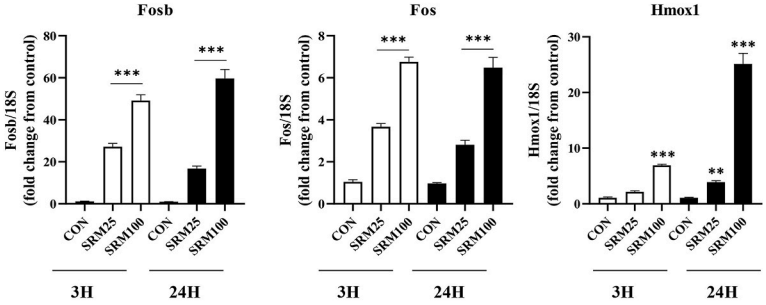

(C)

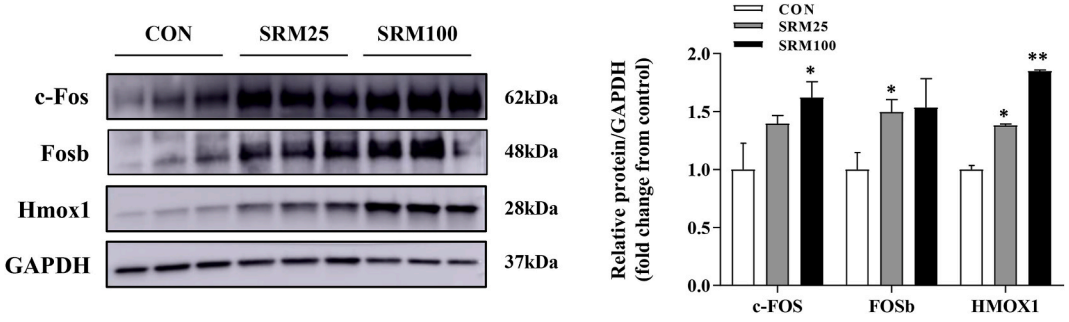

Fig. 5. Identification of co-expressed genes. (A) PPI analysis of five co-expressed differentially expressed genes from the SRM1650b 3 and 24 h treatment groups. (B) Validation of selected gene expression level using qRT-PCR. (C) Validation of protein expression level using Western blot. Uncropped gel images are represented in Fig. S3. Bar graph expressed as the means ± SD of triplicate samples. *p-value<0.05, **p-value<0.01 and *** p-value < 0.001 *vs.* CON (untreated SRM1650b).

the production of HMOX1 [42,43]. However, the molecular mechanism linking Hmox1 induction and ROS generation in H9C2 cells is poorly understood.

Among the 20 differentially upregulated genes in the SRM1650b-treated cells, 2 activator protein (AP-1) family members, Fos and Fosb, were significantly upregulated according to the DEG analysis. Fos is a nuclear phosphoprotein synthesized from mature mRNA derived from the *cFos* gene [44,45] and an immediate early response gene (IEG) in mammalian cells. Transcription factors, such as Fos and Fosb, are subunits of AP-1 that regulate the transcription of specific intracellular genes [46,47]. They bind to the c-Jun/Junb proteins and form an AP-1 dimer. AP-1 is triggered by several external stimuli, such as cytokines, cellular stress, and pathogens [48–50], and coordinates cellular processes, such as cell growth, development, proliferation, inflammation, and cell death [51–53].

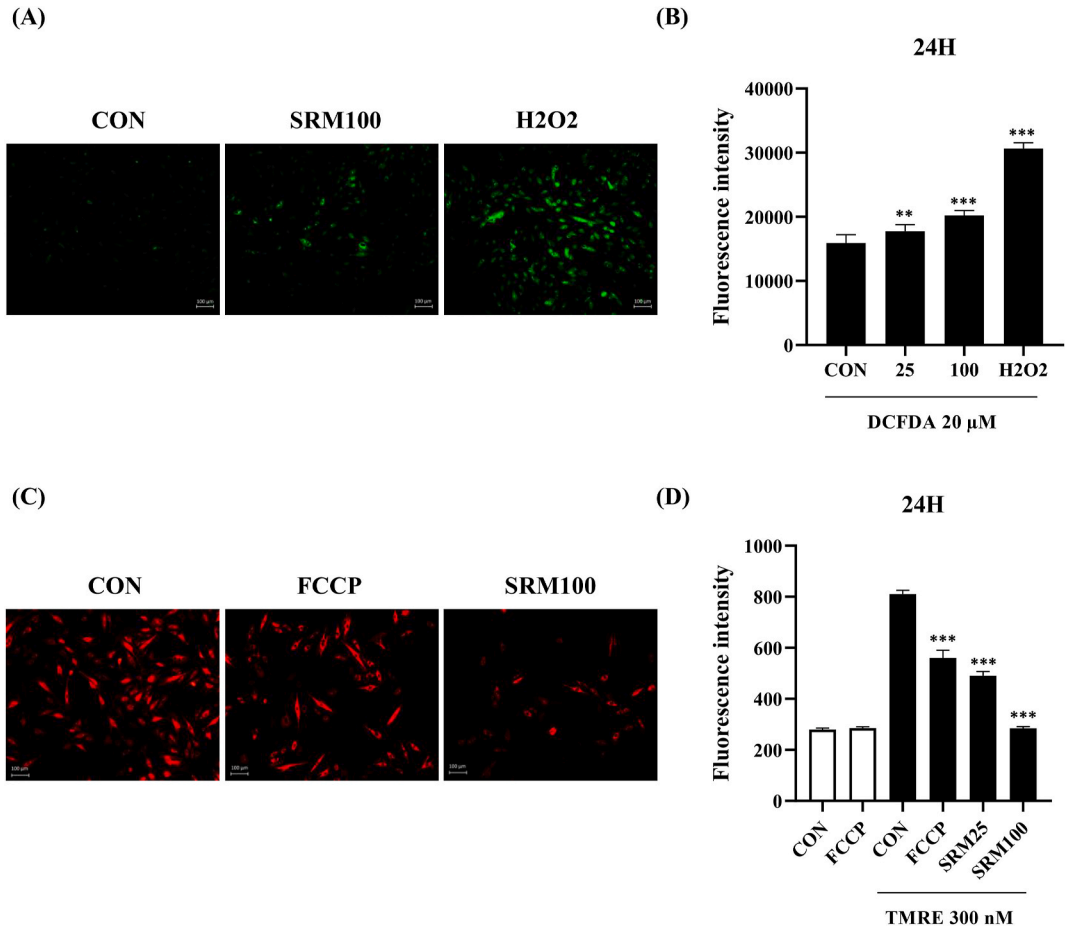

Fig. 6. DCFDA and TMRE fluorescence intensity measured via microscopy and microplate reader. (A) Cells were treated with SRM1650b for 24 h and DCFDA (20 μM) for an additional 30 min before taking the microphotographs. Representative microphotographs showing ROS production in H9C2 cells (FITC filter, 10× magnification, scale bar; 100 μm). (B) Fluorescence intensity measured using microplate reader. H_2O_2, hydrogen peroxide-positive control. (C) Mitochondrial membrane potential measured with TMRE dye staining in H9C2 cells following 24-h treatment with SRM1650b. Representative microphotographs showing TMRE fluorescence in H9C2 cells (rhodamine filter, 10× magnification, scale bar; 100 μm). (D) Fluorescence intensity measured using microplate reader. FCCP, Carbonyl cyanide 4-trifluoromethoxy phenylhydrazone, a mitochondrial oxidative phosphorylation uncoupler. Data are expressed as the means ± SD of triplicate samples. **p-value<0.01 and *** p-value < 0.001 *vs.* CON (untreated SRM).

However, there is a lack of research on the role of AP-1, Fos, and Fosb in H9C2 cells. To the best of our knowledge, this is the first study to demonstrate that *Fos*, *Fosb*, and *Hmox1* serve as significant regulatory genes during SRM1650b exposure of H9C2 cells. The results predict that exposure to SRM1650b induces intracellular oxidative stress, as experimentally confirmed. Moreover, when H9C2 cells were treated with SRM1650b, the expression of Hmox1, Fos, and Fosb was upregulated at both the RNA and protein expression levels (Fig. 5). Therefore, we suggest that the Fos and Fosb proteins activate AP-1 and promote favorable alterations in pro-inflammatory responses to SRM1650b treatment.

5. Conclusions

This study identified genes that were differentially regulated by SRM1650b and conducted a GO analysis of the DEGs. The expression levels of selected genes were validated using qRT-PCR and western blotting assays. Our findings provide novel insights into the molecular mechanisms during SRM1650b exposure. However, the number of samples used for the analysis was small, and the genes involved in cell toxicity were selected at the cellular level, necessitating further analysis of the correlations among genes involved in myocardial disease. In future studies, we intend to select genes involved in myocardial disease by comparing and analyzing the *in vivo* analysis results previously obtained and conducting functional analyses of the selected genes.

Funding

This research did not receive any specific grant from funding agencies in the public, commercial, or not-for-profit sectors.

Data availability statement

Data will be made available on request.

CRediT authorship contribution statement

Kyoung Jin Nho: Writing – review & editing, Writing – original draft, Investigation, Data curation, Conceptualization. **Jae Hoon Shin:** Resources. **Jin Ee Baek:** Investigation. **Sung Won Choi:** Investigation.

Declaration of competing interest

The authors declare that they have no known competing financial interests or personal relationships that could have appeared to influence the work reported in this paper.

Acknowledgements

We would like to thank Editage (www.editage.co.kr) for English language editing.

Appendix A. Supplementary data

Supplementary data to this article can be found online at https://doi.org/10.1016/j.heliyon.2024.e38082.

References

[1] World Health Organization (WHO), Cardiovasc. Dis, WHO Regional Office for Europe, 2019.
[2] K. Shkirkova, K. Lamorie-Foote, M. Connor, A. Patel, G. Barisano, H. Baertsch, Q. Liu, T.E. Morgan, C. Sioutas, W.J. Mack, Effects of ambient particulate matter on vascular tissue: a review, J. Toxicol. Environ. Health B Crit. Rev. 23 (2020) 319–350, https://doi.org/10.1080/10937404.2020.1822971.
[3] J. de Bont, S. Jaganathan, M. Dahlquist, A. Persson, M. Stafoggia, P. Ljungman, Ambient air pollution and cardiovascular diseases: an umbrella review of systematic reviews and meta-analyses, J. Intern. Med. 291 (2022) 779–800, https://doi.org/10.1111/joim.13467.
[4] R.D. Brook, B. Franklin, W. Cascio, Y. Hong, G. Howard, M. Lipsett, R. Luepker, M. Mittleman, J. Samet, S.C. Jr, Smith, I. Tager, Air pollution and cardiovascular disease: a statement for healthcare professionals from the expert panel on population and prevention science of the American heart association, Circulation 109 (2004) 2655–2671, https://doi.org/10.1161/01.CIR.0000128587.30041.C8.
[5] L. Morawska, Z. Ristovski, E.R. Jayaratne, D.U. Keogh, X. Ling, Ambient Nano and ultrafine particles from motor vehicle emissions: characteristics, ambient processing and implications on human exposure, Atmos. Environ. 42 (2008) 8113–8138, https://doi.org/10.1016/j.atmosenv.2008.07.050.
[6] P. Thangavel, D. Park, Y.C. Lee, Recent insights into particulate matter ($PM_{2.5}$)- mediated toxicity in humans: an overview, Int. J. Environ. Res. Publ. Health 19 (2022) 7511, https://doi.org/10.3390/ijerph19127511.
[7] IARC Working Group on the Evaluation of Carcinogenic Risks to Humans, Diesel and gasoline engine exhausts and some nitroarenes, IARC Monogr. Eval. Carcinog. Risks Hum. 105 (2014) 9. IARC monographs on the evaluation of carcinogenic risks to humans.
[8] K. Rumchev, D.V. Hoang, A. Lee, Trends in exposure to diesel particulate matter and prevalence of respiratory symptoms in Western Australian miners, Int. J. Environ. Res. Publ. Health 17 (2020) 8435, https://doi.org/10.3390/ijerph17228435.
[9] M. de Homdedeu, M. Cruz, S. Sanchez-Díez, S.I. Ojanguren, C. Romero-Mesones, J. Vanoribeek, G. Vande Velde, X. Munoz, The immunomodulatory effects of diesel exhaust particles in asthma, Environ. Pollut. 263 (2020) 114600, https://doi.org/10.1016/j.envpol.2020.114600.
[10] M. Kaur, J. Chandel, J. Malik, A.S. Naura, Particulate matter in COPD pathogenesis: an overview, Inflamm. Res. 71 (2022) 797–815, https://doi.org/10.1007/s00011-022-01594-y.
[11] D. Yue, Q. Zhang, J. Zhang, W. Liu, L. Chen, M. Wang, R. Li, S. Qin, X. Song, Y. Ji, Diesel exhaust PM2.5 greatly deteriorates fibrosis process in pre-existing pulmonary fibrosis via ferroptosis, Environ. Int. 171 (2023) 107706, https://doi.org/10.1016/j.envint.2022.107706.
[12] C.A. Pope, R.T. Burnett, G.D. Thurston, M.J. Thun, E.E. Calle, D. Krewski, J.J. Godleski, Cardiovascular mortality and long-term exposure to particulate air pollution: epidemiological evidence of general pathophysiological pathways of disease, Circulation 109 (2004) 71–77, https://doi.org/10.1161/01.CIR.0000108927.80044.7F.
[13] S. Costello, M.D. Attfield, J.H. Lubin, A.M. Neophytou, A. Blair, D.M. Brown, P.A. Stewart, R. Vermeulen, E.A. Eisen, D.T. Silverman, Ischemic heart disease mortality and diesel exhaust and respirable dust exposure in the diesel exhaust in Miners Study, Am. J. Epidemiol. 187 (2018) 2623–2632, https://doi.org/10.1093/aje/kwy182.
[14] S. Basith, B. Manavalan, T.H. Shin, C.B. Park, W.S. Lee, J.T. Kim, G. Lee, The impact of fine particulate matter 2.5 on the cardiovascular system: a review of the invisible killer, Nanomaterials 12 (2022) 2656, https://doi.org/10.3390/nano12152656.
[15] S.G. Al-Kindi, R.D. Brook, S. Biswal, S. Rajagopalan, Environmental determinants of cardiovascular disease: lessons learned from air pollution, Nat. Rev. Cardiol. 17 (2020) 656–672, https://doi.org/10.1038/s41569-020-0371-2.
[16] M.R. Miller, Oxidative stress and the cardiovascular effects of air pollution, Free Radic. Biol. Med. 151 (2020) 69–87, https://doi.org/10.1016/j.freeradbiomed.2020.01.004.
[17] G. Traina, E. Bolzacchini, M. Bonini, D. Contini, P. Mantecca, S.M.E. Caimmi, A. Licari, Role of air pollutants mediated oxidative stress in respiratory diseases, Pediatr. Allergy Immunol. 33 (2022) 38–40, https://doi.org/10.1111/pai.13625.
[18] C.R. Marris, S.N. Kompella, M.R. Miller, J.P. Incardona, F. Brette, J.C. Hancox, E. Sørhus, H.A. Shiels, Polyaromatic hydrocarbons in pollution: a heart-breaking matter, J. Physiol. 598 (2020) 227–247, https://doi.org/10.1113/JP278885.
[19] A. Bhatnagar, Cardiovascular effects of particulate air pollution, Annu. Rev. Med. 73 (2022) 393–406, https://doi.org/10.1146/annurev-med-042220-011549.

[20] A. Fiordelisi, P. Piscitelli, B. Trimarco, E. Coscioni, G. Iaccarino, D. Sorriento, The mechanisms of air pollution and particulate matter in cardiovascular diseases, Heart Fail. Rev. 22 (2017) 337–347, https://doi.org/10.1007/s10741-017-9606-7.

[21] H. Wei, D. Wei, S. Yi, F. Zhang, W. Ding, Oxidative stress induced by urban fine particles in cultured EA.hy926 cells, Hum. Exp. Toxicol. 30 (2011) 579–590, https://doi.org/10.1177/0960327110374207.

[22] X. Pan, Y.Y. Gong, Y. Xu, R.A.S. Ariens, M.N. Routledge, Urban particulate matter induces changes in gene expression in vascular endothelial cells that are associated with altered clot structure in vitro, Thromb. Haemost. 118 (2018) 266–278, https://doi.org/10.1160/TH17-05-0362.

[23] S. Liang, J. Zhang, R. Ning, Z. Du, J. Liu, J.W. Batibawa, J. Duan, Z. Sun, The critical role of endothelial function in fine particulate matter-induced atherosclerosis, Part. Fibre Toxicol. 17 (2020) 61, https://doi.org/10.1186/s12989-020-00391-x.

[24] G.H. Bevan, S.G. Al-Kindi, R.G. Brook, T. Münzel, S. Rajagopalan, Ambient air pollution and atherosclerosis: insights into dose, time, and mechanisms, Arterioscler. Thromb. Vasc. Biol. 41 (2021) 628–637, https://doi.org/10.1161/ATVBAHA.120.315219.

[25] A.V. Zima, L.A. Blatter, Redox regulation of cardiac calcium channels and transporters, Cardiovasc. Res. 71 (2006) 310–321, https://doi.org/10.1016/j.cardiores.2006.02.019.

[26] M. Seddon, Y.H. Looi, A.M. Shah, Oxidative stress and redox signalling in cardiac hypertrophy and heart failure, Heart 93 (2007) 903–907, https://doi.org/10.1136/hrt.2005.068270.

[27] E. Santa-Helena, E.R.D. Calderon, A. Gioda, T.D. Saint Pierre, C.A.N. Gonçalves, A.L. de Castro, B. Jiménez-Vélez, C.R. Santa Gioda, From air to heart: particle pollution (PM2.5) and induced injury on cardioblast cells, Atmos. Pollut. Res. 12 (2021) 152–159, https://doi.org/10.1016/j.apr.2021.03.001.

[28] M. Hong, S. Tao, L. Zhang, L.T. Diao, X. Huang, S. Huang, S.J. Xie, Z.D. Xiao, H. Zhang, RNA sequencing: new technologies and applications in cancer research, J. Hematol. Oncol. 13 (2020), https://doi.org/10.1186/s13045-020-01005-x.

[29] P.D.K. Curry, K.L. Broda, C.J. Carroll, The role of RNA-sequencing as a new genetic diagnosis tool, Curr. Genet. Med. Rep. 9 (2021) 13–21, https://doi.org/10.1007/s40142-021-00199-x.

[30] S.W. Park, S. Park, H.K. Choi, H.J. Park, W. Yu, H.S. Kim, M. Jeon, S.C. Chung, K. Ban, S. Moon, Y.M. Bae, Blue laser-induced selective vasorelaxation by the activation of NOSs, Microvasc. Res. 136 (2021) 104165, https://doi.org/10.1016/j.mvr.2021.104165.

[31] P. Moll, M. Ante, A. Seitz, T. Reda, QuantSeq 3′ mRNA sequencing for RNA quantification, Nat. Methods 11 (2014) i–iii, https://doi.org/10.1038/nmeth.f.376.

[32] A.R. Quinlan, I.M. Hall, BEDTools: a flexible suite of utilities for comparing genomic features, Bioinformatics 26 (2010) 841–842, https://doi.org/10.1093/bioinformatics/btq033.

[33] L.E. González-García, M.N. MacGregor, R.M. Visalakshan, A. Lazarian, A.A. Cavallaro, S. Morsbach, A. Mierczynska-Vasilev, V. Mailänder, K. Landfester, K. Vasilev, Nanoparticles surface chemistry influence on protein corona composition and inflammatory responses, Nanomaterials 12 (2022) 682, https://doi.org/10.3390/nano12040682.

[34] Z. Chen, H. Zhong, J. Wei, S. Lin, Z. Zong, F. Gong, X. Huang, J. Sun, P. Li, H. Lin, B. Wei, J. Chu, Inhibition of Nrf2/HO-1 signaling leads to increased activation of the NLRP3 inflammasome in osteoarthritis, Arthritis Res. Ther. 21 (2019) 300, https://doi.org/10.1186/s13075-019-2085-6.

[35] A. Yachie, Heme Oxygenase-1 deficiency and oxidative stress: a review of 9 independent human cases and animal models, Int. J. Mol. Sci. 22 (2021) 1514, https://doi.org/10.3390/ijms22041514.

[36] J.A. Alonso-Piñeiro, A. Gonzalez-Rovira, I. Sánchez-Gomar, J.A. Moreno, M.C. Durán-Ruiz, Nrf2 and heme Oxygenase-1 involvement in atherosclerosis related oxidative stress, Antioxidants 10 (2021) 1463, https://doi.org/10.3390/antiox10091463.

[37] S.K. Chiang, S.E. Chen, L.C. Chang, The role of HO-1 and its crosstalk with oxidative stress in cancer cell survival, Cells 10 (2021) 2401, https://doi.org/10.3390/cells10092401.

[38] D. Kumar, B.I. Jugdutt, Apoptosis and oxidants in the heart, J. Lab. Clin. Med. 142 (2003) 288–297, https://doi.org/10.1016/S0022-2143(03)00148-3.

[39] M.A. Incalza, R. D'Oria, A. Natalicchio, S. Perrini, L. Laviola, F. Giorgino, Oxidative stress and reactive oxygen species in endothelial dysfunction associated with cardiovascular and metabolic diseases, Vasc. Pharmacol. 100 (2018) 1–19, https://doi.org/10.1016/j.vph.2017.05.005.

[40] H. Bugger, K. Pfeil, Mitochondrial ROS in myocardial ischemia reperfusion and remodeling, Biochim. Biophys. Acta, Mol. Basis Dis. 1866 (2020) 165768, https://doi.org/10.1016/j.bbadis.2020.165768.

[41] R.S. Gangwar, G.H. Bevan, R. Palanivel, L. Das, S. Rajagopalan, Oxidative stress pathways of air pollution mediated toxicity: recent insights, Redox Biol. 34 (2020) 101545, https://doi.org/10.1016/j.redox.2020.101545.

[42] A. Furuyama, S. Hirano, E. Koike, T. Kobayashi, Induction of oxidative stress and inhibition of plasminogen activator inhibitor-1 production in endothelial cells following exposure to organic extracts of diesel exhaust particles and urban fine particles, Arch. Toxicol. 80 (2006) 154–162, https://doi.org/10.1007/s00204-005-0020-x.

[43] S.G. Klein, S. Cambier, J. Hennen, S. Legay, T. Serchi, I. Nelissen, A. Chary, E. Moschini, A. Krein, B. Blömeke, A.C. Gutleb, Endothelial responses of the alveolar barrier in vitro in a dose-controlled exposure to diesel exhaust particulate matter, Part. Fibre Toxicol. 14 (2017) 7, https://doi.org/10.1186/s12989-017-0186-4.

[44] D.G. Herrera, H.A. Robertson, Activation of c-fos in the brain, Prog. Neurobiol. 50 (1996) 83–107, https://doi.org/10.1016/s0301-0082(96)00021-4.

[45] G. Yang, Q. Dong, H. Yang, F. Wang, L. Chen, J. Tang, G. Huang, Y. Zhao, Changes observed in potential key candidate genes of peripheral immunity induced by tai chi among patients with Parkinson's disease, Genes 13 (2022) 1863, https://doi.org/10.3390/genes13101863.

[46] Z. Wu, M. Nicoll, R.J. Ingham, AP-1 family transcription factors: a diverse family of proteins that regulate varied cellular activities in classical hodgkin lymphoma and ALK+ ALCL, Exp. Hematol. Oncol. 10 (2021), https://doi.org/10.1186/s40164-020-00197-9.

[47] P.B. Bhosale, H.H. Kim, A. Abusaliya, P. Vetrivel, S.E. Ha, M.Y. Park, H.J. Lee, G.S. Kim, Structural and functional properties of activator protein-1 in cancer and inflammation, Evid. Based Complement. Alternat. Med. 2022 (2022) 9797929, https://doi.org/10.1155/2022/9797929.

[48] F. Galvagni, M. Orlandini, S. Oliviero, Role of the AP-1 transcription factor FOSL1 in endothelial cells adhesion and migration, Cell Adh. Migr. 7 (2013) 408–411, https://doi.org/10.4161/cam.25894.

[49] Y. Yoshitomi, T. Ikeda, H. Saito-Takatsuji, H. Yonekura, Emerging role of AP-1 transcription factor JunB in angiogenesis and vascular development, Int. J. Mol. Sci. 22 (2021) (2021) 2804, https://doi.org/10.3390/ijms22062804.

[50] A.J. Whitehead, H. Atcha, J.D. Hocker, B. Ren, A.J. Engler, AP-1 signaling modulates cardiac fibroblast stress responses, J. Cell Sci. 136 (2023), https://doi.org/10.1242/jcs.261152 (2023) jcs261152.

[51] M. Karin, Z. Liu, E. Zandi, AP-1 function and regulation, Curr. Opin. Cell Biol. 9 (1997) 240–246, https://doi.org/10.1016/s0955-0674(97)80068-3.

[52] E. Shaulian, M. Karin, AP-1 as a regulator of cell life and death, Nat. Cell Biol. 4 (2002) E131–E136, https://doi.org/10.1038/ncb0502-e131.

[53] X. Yu, Y. Wang, Y. Song, X. Gao, H. Deng, AP-1 is a regulatory transcription factor of inflammaging in the murine kidney and liver, Aging Cell 22 (2023) e13858, https://doi.org/10.1111/acel.13858. (Accessed 8 May 2023).